ACS OMEGA

http://pubs.acs.org/journal/acsodf

Article

Interactions of CO_2 Anion Radicals with Electrolyte Environments from First-Principles Simulations

Morgan M. Cencer,[§] Chenyang Li,[§] Garvit Agarwal, Reginaldo Jose Gomes Neto, Chibueze V. Amanchukwu, and Rajeev S. Assary*

Cite This: *ACS Omega* 2022, 7, 18131−18138

Read Online

ACCESS | Metrics & More | Article Recommendations | Supporting Information

ABSTRACT: Successful transformation of carbon dioxide (CO_2) into value-added products is of great interest, as it contributes in part to the circular carbon economy. Understanding chemical interactions that stabilize crucial reaction intermediates of CO_2 is important, and in this contribution, we employ atom centered density matrix propagation (ADMP) molecular dynamics simulations to investigate interactions between CO_2^- anion radicals with surrounding solvent molecules and electrolyte cations in both aqueous and nonaqueous environments. We show how different cations and solvents affect the stability of the CO_2^- anion radical by examining its angle and distance to a coordinating cation in molecular dynamics simulations. We identify that the strength of CO_2^- interactions can be tailored through choosing an appropriate cation and solvent combination. We anticipate that this fundamental understanding of cation/solvent interactions can facilitate the optimization of a chemical pathway that results from selective stabilization of a crucial reaction intermediate.

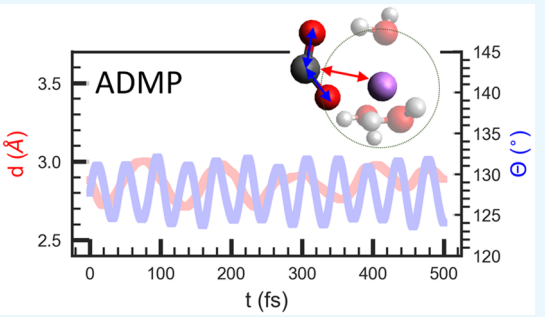

INTRODUCTION

Transforming CO_2 into value-added chemicals or fuels is of great interest to create a sustainable carbon neutral cycle to tackle challenges such as climate change.[1−3] However, reducing CO_2 is a challenging process due to its thermodynamic stability, poor electron affinity, and large kinetic overpotentials. Additionally, as a nonpolar gas, it is only sparingly soluble in water (0.033 M),[4] a common solvent for electrochemical reduction of CO_2.[1] Therefore, it might be advantageous to use nonaqueous (aprotic) solvents due to the higher CO_2 solubility, enhanced potential window, as well as lower proton concentrations that can suppress the undesired hydrogen evolution reaction.[5−7]

The first step of the CO_2 reduction reaction (CO_2RR) involves the formation of CO_2^-, and although successful studies have been performed to unravel the mechanism of electrochemical CO_2RR,[8−17] molecular-level understanding of the dynamics of CO_2^- interacting with surrounding electrolyte cations and solvents (aqueous vs nonaqueous) remains unclear. Of particular interest is the cation effect,[18−24] which was first introduced by Murata and Hori, and it has been better understood that coupling alkali metal cations (M^+) with CO_2^- cocatalyzes the first step[25,26] in aqueous solvents, i.e., * + CO_2 + M^+ + e^- → $M^+\cdots{}^*CO_2^-$ by a short-range electrostatic interaction. In nonaqueous solvents, however, alkali metals are known to inhibit CO_2 reduction due to the formation of a passivation layer containing carbonate species.[27,28] Therefore, electrolyte cations such as NX_4^+ (X = methyl, ethyl, and butyl groups) are being used, and their catalytic roles were examined.[24,29] In aprotic Li−CO_2 batteries, it was argued that a $LiCO_2$ intermediate is crucial to tuning CO_2RR toward a solution- versus surface-mediated pathway.[30]

In this contribution, we aim to provide theoretical insights into the fundamental interactions between CO_2^-, obtained from the electrochemical reduction of CO_2 gas, and the supporting electrolyte cations in various solvents, which will help direct the mechanism toward desired products such as CO, formic acid, and/or oxalate, and will lay a foundation to the future study of specific catalyst systems. Here, we focus on the stabilization effect of the CO_2^- anion radical, as its formation is likely to be the rate-determining step[31] for CO_2 reduction in some aqueous[32−34] and nonaqueous[15,35] media, although this is still under debate.[1] We compare water and nonaqueous solvents (mainly dimethoxyethane (DME) in this work), as glyme-ether-based solvents have been successfully used for electrochemistry (e.g., metal-air/Mg battery) and gas separation processes capturing CO_2[36,37] but have been rarely studied for CO_2 reduction until recently,[27] to the best of our knowledge.

Received: March 22, 2022
Accepted: April 21, 2022
Published: May 17, 2022

https://doi.org/10.1021/acsomega.2c01733
ACS Omega 2022, 7, 18131−18138

To gain understanding of the specific molecular-level interactions, we used *ab initio* molecular dynamics (AIMD) simulations.[38,39] These AIMD simulations show the atomic movement within the system, where the extremes and averages of the oscillations can give detailed information on the stability and other thermodynamic properties. We use the atom centered density matrix propagation (ADMP)[40−42] molecular dynamics method, as it gives the accuracy of density functional theory (DFT) and has advantages particularly around handling the dynamics of charged and radical molecular systems.[43−47] This approach allows us to gather accurate information on how the CO_2^- anion radical interacts with cation and solvent species, based on the computed descriptors such as coordination bond distances (cation−CO_2) and bond angles to develop a fundamental understanding of the interactions. The shorter coordination distance and/or more decreased bond angle of CO_2^- indicate that the intermediate complex can be present for prolonged periods and likely undergo subsequent desired reactions such as chelation, charge transfer interactions, and bond cleavage/formation reactions.[48,49] We further construct a physics-based model to rationalize the relative contributions of electrostatic and covalent/non-covalent interactions to the stabilization effects of CO_2^-.

COMPUTATIONAL DETAILS

Initial geometry optimizations were performed using Gaussian 16 software[50] at the ωb97xD/6-31+G(d,p) level of theory[51,52] with ultrafine integration grids and multiple conformers considered.[53] The frequencies were calculated at the same level of theory. Upon geometry optimization, trajectories were calculated using ADMP molecular dynamics at the ωb97xD/jun-cc-pVDZ level of theory[51,54,55] for 5000 time points (500 fs). ADMP simulations were performed with and without the presence of implicit solvents[56,57] (water (H_2O), tetrahydrofuran (THF), dimethyl sulfoxide (DMSO), acetonitrile (MeCN), and *n*,*n*-dimethylformamide (DMF)). Optimized, maximum, mean, and variation amplitude of the CO_2^- angle (θ) and the CO_2^- distance (to the cation, d) were extracted from the AIMD trajectory. As shown in Figure 1a, the CO_2^- angle (θ) is measured from one oxygen to the other, with the carbon atom as the angle vertex. The CO_2^--to-cation distance (d) is measured from the carbon of the CO_2^- to the center of the cation (either the cation atom or the nitrogen in the ammonium cations). A typical ADMP trajectory is shown in Figure 1b, where CO_2^- oscillates around its equilibrium position over the course of the simulation. Additional details of the simulations are provided in the Supporting Information (SI).

RESULTS AND DISCUSSION

The interaction strength of two charged particles is inversely related to the separating distance.[58] As shown in yellow bars in Figure 1c, based on the simulations, we observe that the interaction of dynamic water molecules increases the cation-to-CO_2^- distance (Δd) for all cations compared to the gas-phase geometry, which manifests less negative complexation energies and binding energies compared to those in the gas phase (ΔH_{gas}, Table 1). Note that the equations for the complexation enthalpy calculations are provided in the Supporting Information. In the case of the DME solvent system, the chelation of the DME molecule with the alkali metal cation increases the interaction distance for alkali metal cations with

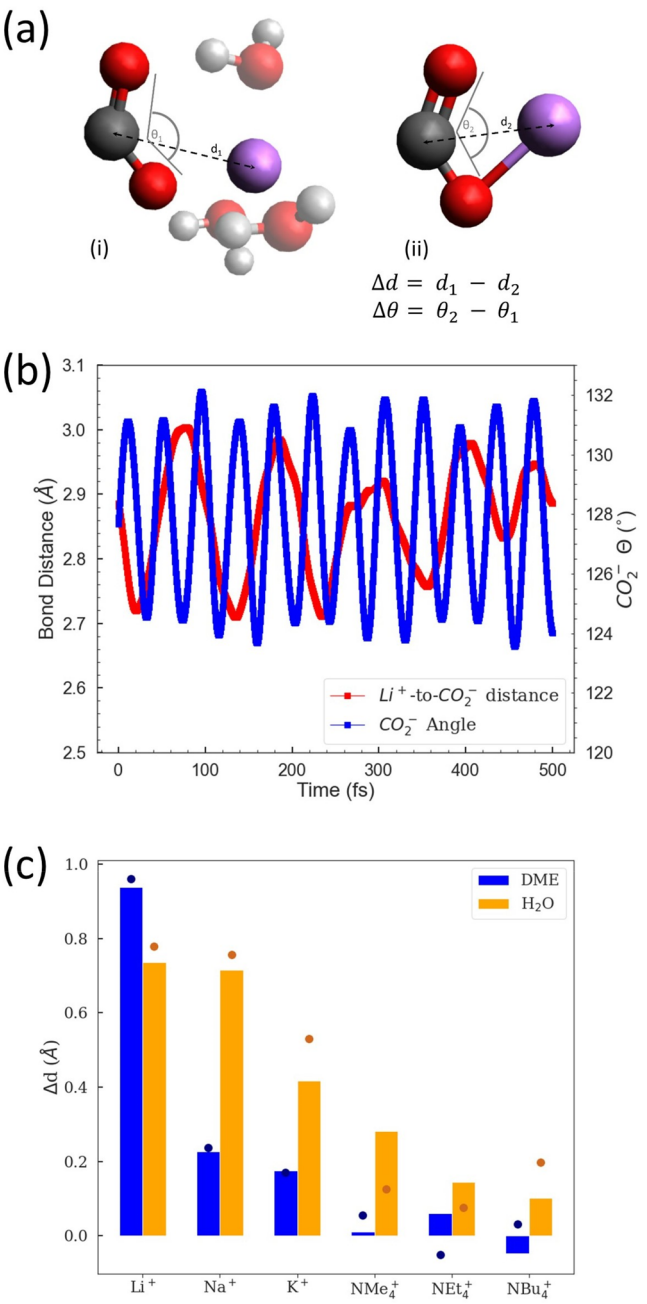

Figure 1. (a) Schematic showing how the change in bond distance (Δd) or change in angle ($\Delta\theta$) is calculated. Scheme (a) shows a molecular cluster with the dashed black line indicating the bond distance (measured Li^+ to CO_2^- from the center of the cation to the carbon atom) and gray lines showing how the bond angle (θ) is measured (with the carbon as the vertex of the angle). The lithium, carbon, oxygen, and hydrogen atoms are shown in purple, dark gray, red, and light gray, respectively. (b) Computed trajectories of the bond distance (Δd) and CO_2^- angle (θ) over 500 fs for a Li^+−CO_2^-−$3H_2O$ molecular cluster. (c) Computed average Δd for various cationic complexes. All complexes in state (i) include three explicit solvent molecules. The dots indicate the difference in bond distances of optimized complexes with and without explicit solvent molecules. Me, Et, and Bu denote methyl, ethyl, and butyl groups, respectively.

the CO_2^-, while for NX_4^+ cations (X = Me, Et, and Bu), the difference is minimal (<0.1 Å). This is largely due to the chemical differences between water and DME molecules. Water molecules are strongly polar and have strong ion-dipole

https://doi.org/10.1021/acsomega.2c01733
ACS Omega 2022, 7, 18131−18138

Table 1. Computed Complexation Enthalpies and Binding Enthalpies ($\Delta H_{complex}$ and BE_{CO2-}, in eV) of CO_2^-, Li^+, Na^+, K^+, and NBu_4^+ with Three Explicit H_2O or DME Molecules

species	$\Delta H_{complex}$ ($3H_2O$)	BE_{CO2-} ($3H_2O$)	$\Delta H_{complex}$ (3DME)	BE_{CO2-} (3DME)	ΔH_{gas} (CO_2^- + M^+)
CO_2^-	−1.72		−1.22		
Li^+	−3.66	−5.08	−5.73	−3.59	−6.50
Na^+	−2.73	−4.96	−4.65	−3.51	−5.66
K^+	−2.03	−4.82	−3.55	−3.49	−5.00
NBu_4^+	−1.17	−3.65	−2.03	−3.28	−3.84

interactions with cations and CO_2^-, as seen from the computed complexation enthalpies ($\Delta H_{complex}$) summarized in Table 1. DME is weakly polar and has chelating interactions with alkali metal cations, where the unshielded positive charge can interact closely with the lone pairs on the oxygen atoms of DME. On the basis of the computed enthalpies of complexation (Table 1), the CO_2^- species itself weakly interacts with DME as compared to water (by 0.50 eV) because DME molecules do not have any strong localized partial positive charges. The NBu_4^+ positive charge is highly shielded by the butyl arms and as such does not closely interact with the DME oxygen atoms, which also can be seen from our quantum chemical calculations that the difference between $\Delta H_{complex}$ and ΔH_{gas} for the NBu_4^+ complex is much smaller than that for alkali metal cations (Table 1). The optimized structures of NBu_4^+ complexes are shown in Figure S1. The optimized structures of Li^+−CO_2^-−solvent with DME and H_2O also corroborate the above analysis; i.e., the oxygen atoms of CO_2^- only bind to Li^+ in the DME solvent, as shown in Figure 2a, whereas in water one of the CO_2^- oxygen atoms binds to Li^+, and the other interacts with water to form an O···H hydrogen bond as shown in Figure 2b. Overall, this suggests that the identity of the supporting electrolyte cation, as well as the polarity of solvents, both dictate the strength of interactions of the CO_2^- anion radical, which primarily consist of (electrostatic) ion-ion and ion-dipole interactions and hydrogen bonds. The different types of interactions will be discussed in more detail.

To further explore how the NX_4^+−CO_2^- interaction responds to the polarity of the solvent, we carried out ADMP simulations with three explicit solvent molecules (in THF, MeCN, DMSO, DMF, and water) and at the same time included the implicit solvent field of corresponding solvent models in Gaussian 16. For these bulky clusters, we repeated each simulation three times with different initial geometries (randomly generated and subsequently optimized) to make sure that the selection of initial structures have no role in dictating the final results. The average and maximum cation-to-CO_2^- distances are shown in Figure 3.

We observe that the strength of interaction between NBu_4^+ and CO_2^- decreases with increasing solvent polarity, indicated by the increasing cation-to-CO_2^- distance, as shown in Figure 3. Such an observation is consistent with the dominant electrostatic interactions and has experimental implications on salt dissociation or formation of ion pairs.[25,27] The positive charge on the NBu_4^+ cation is highly shielded by the bulky and electron donating alkyl chains, which means that changing solvents has a relatively minimal effect on the NBu_4^+. However, the strength of the interaction between CO_2^- and NBu_4^+ is affected by how strongly CO_2^- is coordinated to the solvent and cationic species. Thus, increasing the polarity of the solvent increases CO_2^- coordination with the solvent, weakening the bond between CO_2^- and NBu_4^+. Similar qualitative trends in CO_2RR were also reported by Berto et al.[59] and Shi et al.,[60] where voltammetric experiments in the presence of NBu_4^+ electrolytes have shown larger current density values for CO_2RR in highly polar DMF and MeCN, as compared to low polarity THF. Here, DMSO has the largest standard deviation (Figure 3), which was also found to exhibit the largest deviation from trends due to coordination via the sulfur atom (as opposed to via the oxygen atom in water and THF) in a study of aprotic solvent (THF, DMF, and DMSO) adsorption on metal surfaces by Nørskov and co-workers.[61] In aprotic solvents and NBu_4^+ salts, tailoring the lifetime of the CO_2^- will likely depend on solvent, due to the stabilizing influence of more polar solvents.

The foregoing analysis suggests that both solvents and cations play an important role in the stabilization of the CO_2^- radical,[59,60] but the precise effects are less clear. On the basis of our simulations, we hypothesize that inner-sphere solvation effects are the result of electrostatic and covalent/noncovalent interactions based around solvent stabilization and cation binding, and to this end, we sought to rationalize these by constructing a simple physics-based model. Compared to gas-phase CO_2^-, the introduction of a solvent molecule or a cation reduces the angle of CO_2^-. In Figure 4a, the largest reductions are observed with cations without solvent molecules, following the trend of Li^+ > Na^+ > K^+ > NX_4^+ in the gas phase (gray bars), where X = methyl or longer alkyl groups. There is an overall trend of a larger change in the bond angle ($\Delta\theta$) being

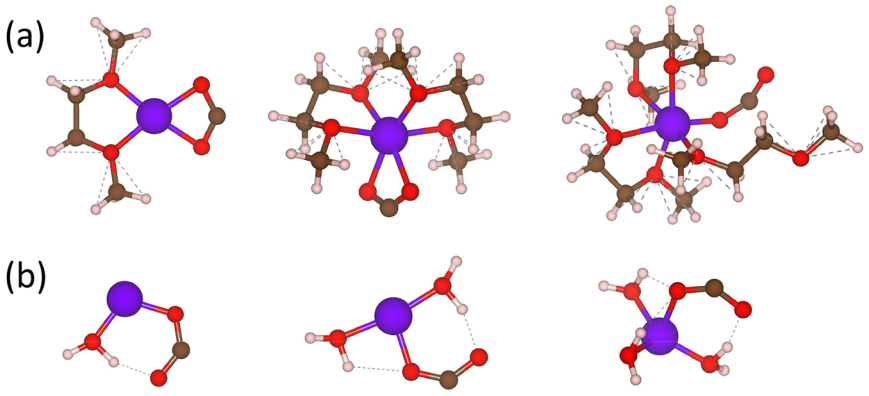

Figure 2. Gas-phase optimized structures of Li^+−CO_2^-−solvent with (a) DME and (b) H_2O.

https://doi.org/10.1021/acsomega.2c01733
ACS Omega 2022, 7, 18131−18138

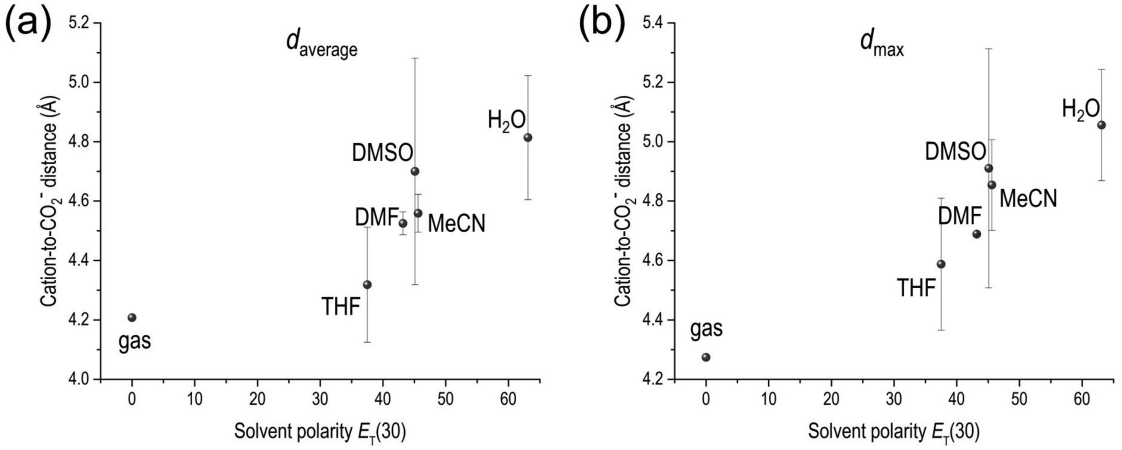

Figure 3. (a) Average cation-to-CO_2^- distance $d_{average}$ and (b) maximum cation-to-CO_2^- distance d_{max} during simulations in various solvents, as plotted against the polarity ($E_T(30)$)[62] of solvent. These data points are for clusters of NBu_4^+, CO_2^-, three molecules of the solvent in question, and with an implicit solvent field of that solvent. Error bars represent standard deviations of three simulations.

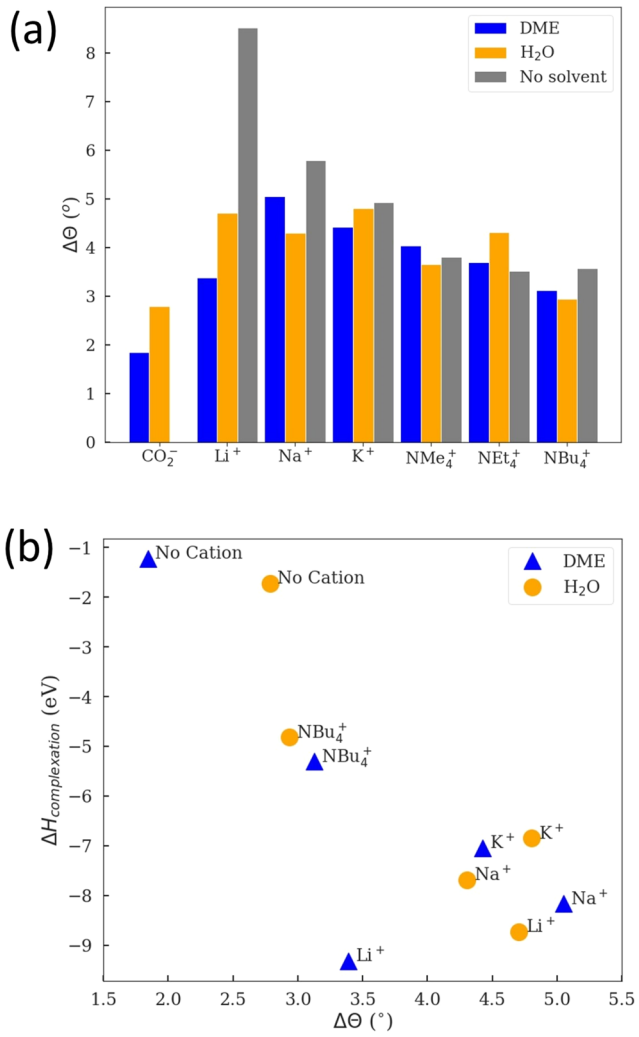

Figure 4. (a) Bar chart of the change in the CO_2^- angle ($\Delta\theta$) between the uncomplexed CO_2^- anion radical in the gas phase and the CO_2^- angle when complexed with cations and/or three solvent molecules. (b) Computed complexation enthalpy plotted against the change in angle from the gas phase to solvated (by DME or H_2O).

associated with more negative complexation enthalpies, as shown in Figure 4b, which also indicates that increased complex stability is associated with a decreased CO_2^- angle. This decreased angle is due to anion radical stabilization through ion-ion interactions, ion-dipole interactions, and/or hydrogen bonds. Given the computed trends of solvent polarity and complexation enthalpy simultaneously (Figure 3 and Figure 4b) and together with known experiment data, we would be able to provide guidance on the electrolyte environments, e.g., with larger stabilizing effects on CO_2^-[63] toward the desired binding.

To decompose the quantum chemistry-calculated complexation enthalpies into stabilization effects by electrostatic ion-ion interactions and/or ion-dipole interactions explicitly, we have constructed a simple physics-based model (see Supporting Information). This model takes in the geometry of a cluster and computes the different types of interactions based on fundamental physics equations. The model-predicted complexation energies against the known DFT-calculated complexation energies are shown in Figure 5, where red triangles ("ion-CO_2^-", e.g., $K^+-CO_2^-$) represent systems that have only electrostatic ion-ion interactions (also see ΔH_{gas} in Table 1), green squares ("ion-solvent", e.g. $NBu_4^+-2H_2O$) represent systems that have ion-dipole and dipole-dipole interactions, and purple circles ("ion-solvent-CO_2^-", e.g., $Li^+-CO_2^--3DME$) represent systems that have ion-ion, ion-dipole, and

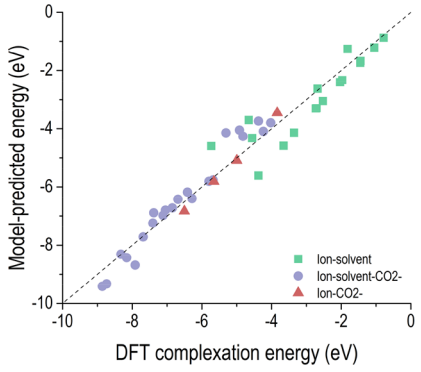

Figure 5. Physics-based model-predicted complexation energy against the known DFT-calculated energy. The dashed line indicates a perfect agreement between the model-predicted complexation energy and the known DFT-calculated complexation energy.

https://doi.org/10.1021/acsomega.2c01733
ACS Omega 2022, 7, 18131−18138

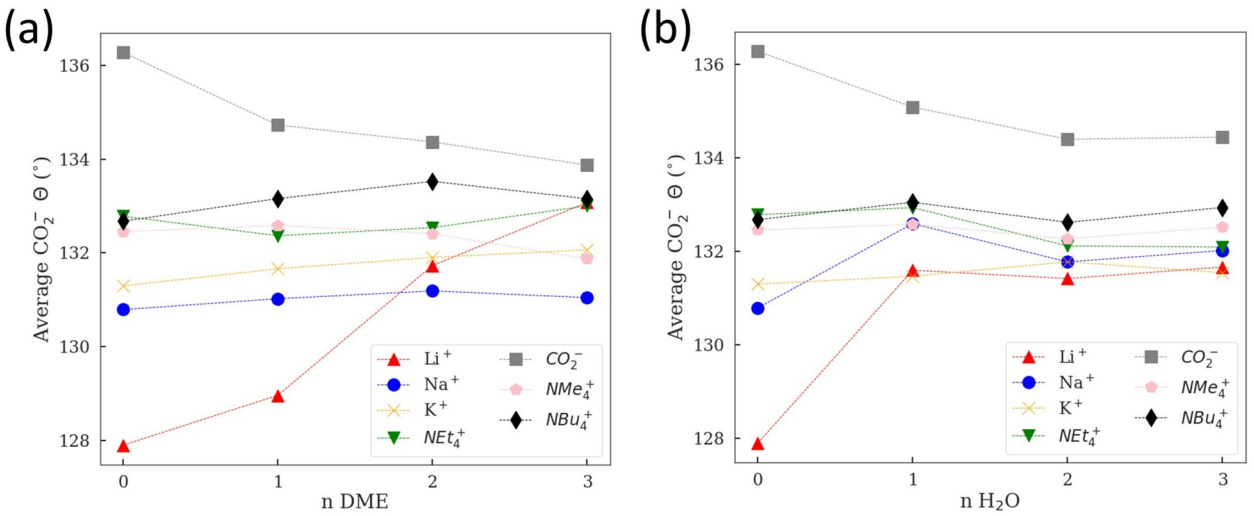

Figure 6. Average CO_2^- angle of different cation−CO_2^-−solvent (DME or H_2O) systems from AIMD simulations: (a) cation−CO_2^-−nDME and (b) cation−CO_2^-−$n H_2O$ (n = 0, 1, 2, 3).

dipole-dipole interactions. The mean absolute error of the model-predicted complexation energy relative to the DFT-calculated value is about 0.12 eV per ion and solvent molecule in a cluster. For all the "ion-solvent-CO_2^-" clusters (purple circles), we calculate that on average 73% of the predicted complexation energy results from the electrostatic ion-ion interactions; likewise, the ion-dipole interaction is much stronger than the dipole-dipole interaction. This indicates that CO_2 activation could be achieved through electrolyte stabilization of the CO_2^- anion product due to a stronger interaction with CO_2^- than the neutral and nonpolar CO_2 gas.[64,65]

Finally, we show the average CO_2^- bond angles in DME and water as a function of the number of solvent molecules (Figure 6) from our simulations. The average cation-to-CO_2^- distances are shown in Figure S2. Here, a small and computationally tractable number of solvent molecules could be used to simulate a reasonable solvation behavior,[66,67] where key interactions between cation/anion and solvent (ion-dipole) are captured. We note that there is a different behavior for Li^+−CO_2^-−nDME where the CO_2^- angle keeps increasing as we increase the number of solvent molecules (Figure 6a). Specifically, for Li^+−CO_2^-−3DME, only one CO_2^- oxygen binds to Li^+ (Figure 2a), resulting in a weak interaction and thus increased angle and increased Li^+-to-CO_2^- distance (by 0.9 Å, see Table 2 and Figure 1c). Such a weakening interaction from bidentate to monodentate geometry is also captured by the physics model. For Li^+−CO_2^-−$n H_2O$ the increased angle and Li^+-to-CO_2^- distance is rather minimal (Table 2 and Figure 6b). These observations are important to keep in mind, as fully solvated systems indicate that the Li^+−CO_2^- interaction is the weakest among alkali metal cations in DME but the strongest in water (Figure S4). However, we know that hard shell Li^+ cation coordinates poorly to an adsorbed CO_2 on the surface,[26] and thus we also compare the relative stability of two configurations of Li^+−CO_2^-−$4H_2O$ (Figure S6) as a function of the partial charge of CO_2, assuming the dominant interaction comes from the electrostatic interaction. We find that for a partial charge of −1e, Li^+ preferably coordinates with CO_2^-, but only within about 0.16 eV compared to the other configuration according to DFT. As the charge of CO_2 is decreased to −0.6e, which mimics its charge state on the surface, we find that Li^+ now preferably coordinates with $4H_2O$ according to our physics-based model (Figure S6).

Table 2. Computed Li^+ Coordination Distances for Complexes with O Atoms (of DME/H_2O) and C Atoms (of CO_2^-)

	d(Li−$O_{solvent}$)/Å	d(Li−C_{CO2-})/Å
Li^+−CO_2^-		1.92
Li^+−CO_2^-−1DME	2.00	2.19
Li^+−CO_2^-−2DME	2.09	2.39
Li^+−CO_2^-−3DME	2.20	3.07
Li^+−CO_2^-−$1H_2O$	1.86	2.63
Li^+−CO_2^-−$2H_2O$	1.93	2.76
Li^+−CO_2^-−$3H_2O$	2.01	2.89

CONCLUSIONS

We have used ADMP simulations to investigate the interactions of the CO_2^- anion radical in various chemical environments, including both aqueous and nonaqueous electrolytes. Simulations show the effect of cations and solvent molecules on the fundamental properties of bond distance and angle of CO_2, e.g., DME solvation increases the interaction distance for small cations with CO_2^-, while for NX_4^+ cations the difference is minimal. This correlates well with the complexation enthalpy of CO_2^-, offering a guide to which combinations of solvent and supporting electrolyte may provide the desired experimental conditions. Moreover, we have shown that the identity of the supporting electrolyte cation will likely matter more in polar solvents than in solvents of less polarity. Therefore, we can tailor the strength of interactions between CO_2^- and supporting electrolytes through the judicious choice of electrolyte cations and solvents. Our simulation and physics-based model provides a general and suitable approach to studying solvation effects particularly in an aprotic electrolyte environment, and it was shown that the electrochemical CO_2RR activity could be correlated to the bulk solvation properties in DME and DMSO.[27] We note the limitation of our model not yet including the electrode surface as well as the pH effect at the

https://doi.org/10.1021/acsomega.2c01733
ACS Omega 2022, 7, 18131−18138

interface,[68] and future experimental and computational efforts are necessary to elucidate the interactions of the CO_2 anion radical with the electrode surface.

■ ASSOCIATED CONTENT

Supporting Information

The Supporting Information is available free of charge at https://pubs.acs.org/doi/10.1021/acsomega.2c01733.

Details of computational methods and analysis, details of quantum chemical calculations and physics-based model, list of systems simulated using ADMP, and trend of cation-to-CO_2^- bond distances and CO_2^- angles (Table S1 and Figures S1−S6) (PDF)

■ AUTHOR INFORMATION

Corresponding Author

Rajeev S. Assary − *Materials Science Division, Argonne National Laboratory, Lemont, Illinois 60439, United States;* orcid.org/0000-0002-9571-3307; Email: assary@anl.gov

Authors

Morgan M. Cencer − *Materials Science Division, Argonne National Laboratory, Lemont, Illinois 60439, United States;* orcid.org/0000-0003-2806-8317

Chenyang Li − *Materials Science Division, Argonne National Laboratory, Lemont, Illinois 60439, United States;* orcid.org/0000-0002-5155-4631

Garvit Agarwal − *Materials Science Division, Argonne National Laboratory, Lemont, Illinois 60439, United States;* Present Address: Schrödinger, Inc., New York, NY 10036; orcid.org/0000-0002-7814-6072

Reginaldo Jose Gomes Neto − *Pritzker School of Molecular Engineering, The University of Chicago, Chicago, Illinois 60637, United States*

Chibueze V. Amanchukwu − *Pritzker School of Molecular Engineering, The University of Chicago, Chicago, Illinois 60637, United States; Chemical Sciences and Engineering Division, Argonne National Laboratory, Lemont, Illinois 60439, United States;* orcid.org/0000-0002-6573-1213

Complete contact information is available at: https://pubs.acs.org/10.1021/acsomega.2c01733

Author Contributions

§M.M.C. and C.L. contributed equally to this work.

Notes

The authors declare no competing financial interest.

■ ACKNOWLEDGMENTS

This work was supported by funding from The University of Chicago Center for Data and Computing (CDAC) program and the Data Science Institute. R.S.A. and C.L. would like to acknowledge Consortium for Computational Physics and Chemistry (CCPC), which is supported by the Bioenergy Technologies Office (BETO) of Energy Efficiency & Renewable Energy (EERE). C.V.A. acknowledges support from the University of Chicago and the Neubauer Family Assistant Professors program. We gratefully acknowledge the computing resources provided on "Bebop", a 1024-node computing cluster operated by the Laboratory Computing Resource Center at the Argonne National Laboratory. We also acknowledge the computational resources from the Center for Nanoscale Materials, an Office of Science user facility, which was supported by the U.S. Department of Energy, Office of Science, Office of Basic Energy Sciences, under Contract No. DE-AC02-06CH11357. The submitted manuscript has been created by UChicago Argonne, LLC, Operator of Argonne National Laboratory ("Argonne"). Argonne, a U.S. Department of Energy Office of Science laboratory, is operated under Contract No. DE-AC02-06CH11357. The U.S. Government retains for itself, and others acting on its behalf, a paid-up nonexclusive, irrevocable worldwide license in said article to reproduce, prepare derivative works, distribute copies to the public, and perform publicly and display publicly, by or on behalf of the Government.

■ REFERENCES

(1) Birdja, Y. Y.; Pérez-Gallent, E.; Figueiredo, M. C.; Göttle, A. J.; Calle-Vallejo, F.; Koper, M. T. M. Advances and Challenges in Understanding the Electrocatalytic Conversion of Carbon Dioxide to Fuels. *Nature Energy* **2019**, *4* (9), 732−745.

(2) De Luna, P.; Hahn, C.; Higgins, D.; Jaffer, S. A.; Jaramillo, T. F.; Sargent, E. H. What Would It Take for Renewably Powered Electrosynthesis to Displace Petrochemical Processes? *Science* **2019**, *364* (6438). DOI: 10.1126/science.aav3506.

(3) Whipple, D. T.; Kenis, P. J. A. Prospects of CO2 Utilization via Direct Heterogeneous Electrochemical Reduction. *J. Phys. Chem. Lett.* **2010**, *1* (24), 3451−3458.

(4) Dean, J. A. *Lange's Handbook of Chemistry*, 15th ed.; Dean, J. A., Ed.; McGraw-Hill, 1999.

(5) Tomita, Y.; Hori, Y. Electrochemical Reduction of Carbon Dioxide at a Platinum Electrode in Acetonitrile-Water Mixtures. *Stud. Surf. Sci. Catal.* **1998**, *114*, 581−584.

(6) Ikeda, S.; Takagi, T.; Ito, K. Selective Formation of Formic Acid, Oxalic Acid, and Carbon Monoxide by Electrochemical Reduction of Carbon Dioxide. *Bull. Chem. Soc. Jpn.* **1987**, *60*, 2517−2522.

(7) König, M.; Vaes, J.; Klemm, E.; Pant, D. Solvents and Supporting Electrolytes in the Electrocatalytic Reduction of CO_2. *iScience* **2019**, *19*, 135−160.

(8) Resasco, J.; Chen, L. D.; Clark, E.; Tsai, C.; Hahn, C.; Jaramillo, T. F.; Chan, K.; Bell, A. T. Promoter Effects of Alkali Metal Cations on the Electrochemical Reduction of Carbon Dioxide. *J. Am. Chem. Soc.* **2017**, *139* (32), 11277−11287.

(9) Murata, A.; Hori, Y. Product Selectivity Affected by Cationic Species in Electrochemical Reduction of CO2 and CO at a Cu Electrode. *Bull. Chem. Soc. Jpn.* **1991**, *64*, 123−127.

(10) Thorson, M. R.; Siil, K. I.; Kenis, P. J. A. Effect of Cations on the Electrochemical Conversion of CO 2 to CO. *J. Electrochem. Soc.* **2013**, *160* (1), F69−F74.

(11) Singh, M. R.; Kwon, Y.; Lum, Y.; Ager, J. W.; Bell, A. T. Hydrolysis of Electrolyte Cations Enhances the Electrochemical Reduction of CO2 over Ag and Cu. *J. Am. Chem. Soc.* **2016**, *138* (39), 13006−13012.

(12) Cheng, T.; Fortunelli, A.; Goddard, W. A. Reaction Intermediates during Operando Electrocatalysis Identified from Full Solvent Quantum Mechanics Molecular Dynamics. *Proc. Natl. Acad. Sci. U. S. A.* **2019**, *116* (16), 7718−7722.

(13) Ma, M.; Liu, K.; Shen, J.; Kas, R.; Smith, W. A. In Situ Fabrication and Reactivation of Highly Selective and Stable Ag Catalysts for Electrochemical CO_2 Conversion. *ACS Energy Letters* **2018**, *3* (6), 1301−1306.

(14) Schreier, M.; Yoon, Y.; Jackson, M. N.; Surendranath, Y. Competition between H and CO for Active Sites Governs Copper-Mediated Electrosynthesis of Hydrocarbon Fuels. *Angewandte Chemie - International Edition* **2018**, *57* (32), 10221−10225.

(15) Gennaro, A.; Isse, A. A.; Severin, M. G.; Vianello, E.; Bhugun, I.; Savéant, J. M. Mechanism of the Electrochemical Reduction of Carbon Dioxide at Inert Electrodes in Media of Low Proton Availability. *Journal of the Chemical Society - Faraday Transactions* **1996**, *92* (20), 3963−3968.

(16) Ludwig, T.; Singh, A. R.; Nørskov, J. K. Acetonitrile Transition Metal Interfaces from First Principles. *J. Phys. Chem. Lett.* **2020**, *11* (22), 9802−9811.
(17) Cao, L.; Raciti, D.; Li, C.; Livi, K. J. T.; Rottmann, P. F.; Hemker, K. J.; Mueller, T.; Wang, C. Mechanistic Insights for Low-Overpotential Electroreduction of CO_2 to CO on Copper Nanowires. *ACS Catal.* **2017**, *7* (12), 8578−8587.
(18) Kyriacou, D.; Jahngen, E. G. E. An Electrogenerative Acidobasic Cell Utilizing Biomass for the Generation of Electricity and Molecular Hydrogen. *J. Appl. Electrochem.* **1993**, *23* (11), 1196−1198.
(19) Moura de Salles Pupo, M.; Kortlever, R. Electrolyte Effects on the Electrochemical Reduction of CO_2. *ChemPhysChem* **2019**, *20* (22), 2926−2935.
(20) Kim, H.-Y.; Choi, I.; Ahn, S. H.; Hwang, S. J.; Yoo, S. J.; Han, J.; Kim, J.; Park, H.; Jang, J. H.; Kim, S.-K. Analysis on the Effect of Operating Conditions on Electrochemical Conversion of Carbon Dioxide to Formic Acid. *Int. J. Hydrogen Energy* **2014**, *39* (29), 16506−16512.
(21) Ringe, S.; Clark, E. L.; Resasco, J.; Walton, A.; Seger, B.; Bell, A. T.; Chan, K. Understanding Cation Effects in Electrochemical CO_2 Reduction. *Energy Environ. Sci.* **2019**, *12* (10), 3001−3014.
(22) Gunathunge, C. M.; Ovalle, V. J.; Waegele, M. M. Probing Promoting Effects of Alkali Cations on the Reduction of CO at the Aqueous Electrolyte/Copper Interface. *Phys. Chem. Chem. Phys.* **2017**, *19* (44), 30166−30172.
(23) Verma, S.; Lu, X.; Ma, S.; Masel, R. I.; Kenis, P. J. A. The Effect of Electrolyte Composition on the Electroreduction of CO_2 to CO on Ag Based Gas Diffusion Electrodes. *Phys. Chem. Chem. Phys.* **2016**, *18* (10), 7075−7084.
(24) Berto, T. C.; Zhang, L.; Hamers, R. J.; Berry, J. F. Electrolyte Dependence of CO_2 Electroreduction: Tetraalkylammonium Ions Are Not Electrocatalysts. *ACS Catal.* **2015**, *5* (2), 703−707.
(25) Shin, S.-J.; Choi, H.; Ringe, S.; Won, D. H.; Choi, C. H.; Kim, H. Alkali Cation Effect on CO_2 Electroreduction to CO: A Local Colligative Property. *ChemRxiv* **2021**, DOI: 10.26434/chemrxiv-2021-x0msb-v2
(26) Monteiro, M. C. O.; Dattila, F.; Hagedoorn, B.; García-Muelas, R.; López, N.; Koper, M. T. M. Absence of CO_2 Electroreduction on Copper, Gold and Silver Electrodes without Metal Cations in Solution. *Nature Catalysis* **2021**, *4* (8), 654−662.
(27) Gomes, R. J.; Birch, C.; Cencer, M. M.; Li, C.; Son, S.; Bloom, D.; Assary, R. S.; Amanchukwu, C. V. Probing Electrolyte Influence on CO 2 Reduction in Aprotic Solvents. *ChemRxiv* **2021**, 10.26434/chemrxiv-2021-17zmv. DOI: 10.26434/chemrxiv-2021-17zmv
(28) Xie, Z.; Zhang, X.; Zhang, Z.; Zhou, Z. Metal-CO2 Batteries on the Road: CO2 from Contamination Gas to Energy Source. *Adv. Mater.* **2017**, *29* (15), 1605891.
(29) Lamy, E.; Nadjo, L.; Saveant, J. M. Standard Potential and Kinetic Parameters of the Electrochemical Reduction of Carbon Dioxide in Dimethylformamide. *Journal of Electroanalytical Chemistry and Interfacial Electrochemistry* **1977**, *78* (2), 403−407.
(30) Zhao, Z.; Wang, E.; Wang, J.; Liu, C.; Peng, Z. Kinetics of the CO_2 Reduction Reaction in Aprotic Li-CO_2 Batteries: A Model Study. *Journal of Materials Chemistry A* **2021**, *9* (6), 3290−3296.
(31) Wuttig, A.; Yaguchi, M.; Motobayashi, K.; Osawa, M.; Surendranath, Y. Inhibited Proton Transfer Enhances Au-Catalyzed CO2-to-Fuels Selectivity. *Proc. Natl. Acad. Sci. U. S. A.* **2016**, *113* (32), E4585−E4593.
(32) Verma, S.; Hamasaki, Y.; Kim, C.; Huang, W.; Lu, S.; Jhong, H. R. M.; Gewirth, A. A.; Fujigaya, T.; Nakashima, N.; Kenis, P. J. A. Insights into the Low Overpotential Electroreduction of CO2 to CO on a Supported Gold Catalyst in an Alkaline Flow Electrolyzer. *ACS Energy Letters* **2018**, *3* (1), 193−198.
(33) Dunwell, M.; Luc, W.; Yan, Y.; Jiao, F.; Xu, B. Understanding Surface-Mediated Electrochemical Reactions: CO2 Reduction and Beyond. *ACS Catal.* **2018**, *8* (9), 8121−8129.
(34) Zhang, B. A.; Ozel, T.; Elias, J. S.; Costentin, C.; Nocera, D. G. Interplay of Homogeneous Reactions, Mass Transport, and Kinetics in Determining Selectivity of the Reduction of CO2 on Gold Electrodes. *ACS Central Science* **2019**, *5* (6), 1097−1105.
(35) Amatore, C.; Savéant, J. M. Mechanism and Kinetic Characteristics of the Electrochemical Reduction of Carbon Dioxide in Media of Low Proton Availability. *J. Am. Chem. Soc.* **1981**, *103* (17), 5021−5023.
(36) Vardar, G.; Smith, J. G.; Thompson, T.; Inagaki, K.; Naruse, J.; Hiramatsu, H.; Sleightholme, A. E. S.; Sakamoto, J.; Siegel, D. J.; Monroe, C. W. Mg/O2 Battery Based on the Magnesium-Aluminum Chloride Complex (MACC) Electrolyte. *Chem. Mater.* **2016**, *28* (21), 7629−7637.
(37) Gutiérrez, A.; Atilhan, M.; Aparicio, S. Molecular Modeling Analysis of CO2 Absorption by Glymes. *J. Phys. Chem. B* **2018**, *122* (6), 1948−1957.
(38) Kohn, W.; Sham, L. J. Self-Consistent Equations Including Exchange and Correlation Effects. *Phys. Rev.* **1965**, *140* (4A), A1133.
(39) Hohenberg, P.; Kohn, W. Inhomogeneous Electron Gas. *Phys. Rev.* **1964**, *136* (3B), B864.
(40) Iyengar, S. S.; Schlegel, H. B.; Millam, J. M.; Voth, G. A.; Scuseria, G. E.; Frisch, M. J. Ab Initio Molecular Dynamics: Propagating the Density Matrix with Gaussian Orbitals. II. Generalizations Based on Mass-Weighting, Idempotency, Energy Conservation and Choice of Initial Conditions. *J. Chem. Phys.* **2001**, *115* (22), 10291−10302.
(41) Schlegel, H. B.; Iyengar, S. S.; Li, X.; Millam, J. M.; Voth, G. A.; Scuseria, G. E.; Frisch, M. J. Ab Initio Molecular Dynamics: Propagating the Density Matrix with Gaussian Orbitals. III. Comparison with Born-Oppenheimer Dynamics. *J. Chem. Phys.* **2002**, *117* (19), 8694−8704.
(42) Schlegel, H. B.; Millam, J. M.; Iyengar, S. S.; Voth, G. A.; Daniels, A. D.; Scuseria, G. E.; Frisch, M. J. Ab Initio Molecular Dynamics: Propagating the Density Matrix with Gaussian Orbitals. *J. Chem. Phys.* **2001**, *114* (22), 9758−9763.
(43) McDonnell, M.; Laforge, A. C.; Reino-González, J.; Disla, M.; Kling, N. G.; Mishra, D.; Obaid, R.; Sundberg, M.; Svoboda, V.; Díaz-Tendero, S.; Martín, F.; Berrah, N. Ultrafast Laser-Induced Isomerization Dynamics in Acetonitrile. *J. Phys. Chem. Lett.* **2020**, *11* (16), 6724−6729.
(44) Barreiro-Lage, D.; Bolognesi, P.; Chiarinelli, J.; Richter, R.; Zettergren, H.; Stockett, M. H.; Carlini, L.; Diaz-Tendero, S.; Avaldi, L. smart Decomposition" of Cyclic Alanine-Alanine Dipeptide by VUV Radiation: A Seed for the Synthesis of Biologically Relevant Species. *J. Phys. Chem. Lett.* **2021**, *12* (30), 7379−7386.
(45) Esteban-Gómez, D.; Cassino, C.; Botta, M.; Platas-Iglesias, C. 17O and 1H Relaxometric and DFT Study of Hyperfine Coupling Constants in $[Mn(H_2O)6]2+$. *RSC Adv.* **2014**, *4* (14), 7094−7103.
(46) Iyengar, S. S. Dynamical Effects on Vibrational and Electronic Spectra of Hydroperoxyl Radical Water Clusters. *J. Chem. Phys.* **2005**, *123* (8), 084310.
(47) Zhang, Y.; Xu, Z.; Zhao, Y.; Zhang, X. Ab Initio Molecular Dynamics Simulation Study of Dissociation Electron Attachment to Lactic Acid and Isomer. *Sci. Rep.* **2019**, *9* (1), 1−11.
(48) Chernyshova, I. V.; Somasundaran, P.; Ponnurangam, S. On the Origin of the Elusive First Intermediate of CO2 Electroreduction. *Proc. Natl. Acad. Sci. U. S. A.* **2018**, *115* (40), E9261−E9270.
(49) Jestilä, J. S.; Denton, J. K.; Perez, E. H.; Khuu, T.; Aprà, E.; Xantheas, S. S.; Johnson, M. A.; Uggerud, E. Characterization of the Alkali Metal Oxalates (MC2O4-) and Their Formation by CO2 Reduction: Via the Alkali Metal Carbonites (MCO2-). *Phys. Chem. Chem. Phys.* **2020**, *22* (14), 7460−7473.
(50) Frisch, M. J.; Trucks, G. W.; Schlegel, H. B.; Scuseria, G. E.; Robb, M. A.; Cheeseman, J. R.; Scalmani, G.; Barone, V.; Petersson, G. A.; Nakatsuji, H.; Li, X.; Caricato, M.; Marenich, A. V.; Bloino, J.; Janesko, B. G.; Gomperts, R.; Mennucci, B.; Hratchian, H. P.; Ortiz, J. V.; Izmaylov, A. F.; Sonnenberg, J. L.; Williams-Young, D.; Ding, F.; Lipparini, F.; Egidi, F.; Goings, J.; Peng, B.; Petrone, A.; Henderson, T.; Ranasinghe, D.; Zakrzewski, V. G.; Gao, J.; Rega, N.; Zheng, G.; Liang, W.; Hada, M.; Ehara, M.; Toyota, K.; Fukuda, R.; Hasegawa, J.; Ishida, M.; Nakajima, T.; Honda, Y.; Kitao, O.; Nakai, H.; Vreven, T.;

https://doi.org/10.1021/acsomega.2c01733
ACS Omega 2022, 7, 18131−18138

Throssell, K.; Montgomery, J. A., Jr.; Peralta, J. E.; Ogliaro, F.; Bearpark, M. J.; Heyd, J. J.; Brothers, E. N.; Kudin, K. N.; Staroverov, V. N.; Keith, T. A.; Kobayashi, R.; Normand, J.; Raghavachari, K.; Rendell, A. P.; Burant, J. C.; Iyengar, S. S.; Tomasi, J.; Cossi, M.; Millam, J. M.; Klene, M.; Adamo, C.; Cammi, R.; Ochterski, J. W.; Martin, R. L.; Morokuma, K.; Farkas, O.; Foresman, J. B.; Fox, D. J. *Gaussian 16*, Revision A.03; Gaussian Inc.: Wallingford, CT, 2016.

(51) Chai, J. Da; Head-Gordon, M. Long-Range Corrected Hybrid Density Functionals with Damped Atom-Atom Dispersion Corrections. *Phys. Chem. Chem. Phys.* **2008**, *10* (44), 6615−6620.

(52) Petersson, G. A.; Bennett, A.; Tensfeldt, T. G.; Al-Laham, M. A.; Shirley, W. A.; Mantzaris, J. A Complete Basis Set Model Chemistry. I. The Total Energies of Closed-Shell Atoms and Hydrides of the First-Row Elements. *J. Chem. Phys.* **1988**, *89* (4), 2193−2218.

(53) Martínez, L.; Andrade, R.; Birgin, E. G.; Martínez, J. M. PACKMOL: A Package for Building Initial Configurations for Molecular Dynamics Simulations. *J. Comput. Chem.* **2009**, *30* (13), 2157−2164.

(54) Papajak, E.; Zheng, J.; Xu, X.; Leverentz, H. R.; Truhlar, D. G. Perspectives on Basis Sets Beautiful: Seasonal Plantings of Diffuse Basis Functions. *J. Chem. Theory Comput.* **2011**, *7* (10), 3027−3034.

(55) Woon, D. E.; Dunning, T. H. Gaussian Basis Sets for Use in Correlated Molecular Calculations. V. Core-Valence Basis Sets for Boron through Neon. *J. Chem. Phys.* **1995**, *103* (11), 4572−4585.

(56) Cossi, M.; Rega, N.; Scalmani, G.; Barone, V. Energies, Structures, and Electronic Properties of Molecules in Solution with the C-PCM Solvation Model. *J. Comput. Chem.* **2003**, *24* (6), 669−681.

(57) Barone, V.; Cossi, M. Quantum Calculation of Molecular Energies and Energy Gradients in Solution by a Conductor Solvent Model. *J. Phys. Chem. A* **1998**, *102* (11), 1995−2001.

(58) Lindgren, E. B.; Chan, H. K.; Stace, A. J.; Besley, E. Progress in the Theory of Electrostatic Interactions between Charged Particles. *Phys. Chem. Chem. Phys.* **2016**, *18* (8), 5883−5895.

(59) Berto, T. C.; Zhang, L.; Hamers, R. J.; Berry, J. F. Electrolyte Dependence of CO2 Electroreduction: Tetraalkylammonium Ions Are Not Electrocatalysts. *ACS Catal.* **2015**, *5* (2), 703−707.

(60) Shi, J.; Shen, F. x.; Shi, F.; Song, N.; Jia, Y. J.; Hu, Y. Q.; Li, Q. Y.; Liu, J. x.; Chen, T. Y.; Dai, Y. N. Electrochemical Reduction of CO_2 into CO in Tetrabutylammonium Perchlorate/Propylene Carbonate: Water Effects and Mechanism. *Electrochim. Acta* **2017**, *240*, 114−121.

(61) Ludwig, T.; Singh, A. R.; Nørskov, J. K. Nonaqueous Solvent Adsorption on Transition Metal Surfaces with Density Functional Theory: Interaction OfN,N-Dimethylformamide (DMF), Tetrahydrofuran (THF), and Dimethyl Sulfoxide (DMSO) with Ag, Cu, Pt, Rh, and Re Surfaces. *J. Phys. Chem. C* **2021**, *125* (40), 21943−21957.

(62) Cerõn-Carrasco, J. P.; Jacquemin, D.; Laurence, C.; Planchat, A.; Reichardt, C.; Sraïdi, K. Solvent Polarity Scales: Determination of New ET(30) Values for 84 Organic Solvents. *J. Phys. Org. Chem.* **2014**, *27* (6), 512−518.

(63) Monteiro, M. C. O.; Dattila, F.; Hagedoorn, B.; García-Muelas, R.; López, N.; Koper, M. T. M. Absence of CO2 Electroreduction on Copper, Gold and Silver Electrodes without Metal Cations in Solution. *Nature Catalysis* **2021**, *4* (8), 654−662.

(64) Li, G.; Wang, B.; Resasco, D. E. Water-Mediated Heterogeneously Catalyzed Reactions. *ACS Catal.* **2020**, *10* (2), 1294−1309.

(65) Sato, S.; Saita, K.; Sekizawa, K.; Maeda, S.; Morikawa, T. Low-Energy Electrocatalytic CO $_2$ Reduction in Water over Mn-Complex Catalyst Electrode Aided by a Nanocarbon Support and K^+ Cations. *ACS Catal.* **2018**, *8* (5), 4452−4458.

(66) Mills, J. N.; McCrum, I. T.; Janik, M. J. Alkali Cation Specific Adsorption onto Fcc(111) Transition Metal Electrodes. *Phys. Chem. Chem. Phys.* **2014**, *16* (27), 13699−13707.

(67) Nie, X.; Luo, W.; Janik, M. J.; Asthagiri, A. Reaction Mechanisms of CO_2 Electrochemical Reduction on Cu(1 1 1) Determined with Density Functional Theory. *J. Catal.* **2014**, *312*, 108−122.

(68) Ayemoba, O.; Cuesta, A. Spectroscopic Evidence of Size-Dependent Buffering of Interfacial PH by Cation Hydrolysis during CO_2 Electroreduction. *ACS Appl. Mater. Interfaces* **2017**, *9* (33), 27377−27382.

https://doi.org/10.1021/acsomega.2c01733
ACS Omega 2022, 7, 18131−18138